Preprints, 10th IFAC International Symposium on
Advances in Automotive Control
Columbus, Ohio, USA, August 28-30, 2022

Energy Management for RCCI Engines with Electrically-Assisted Turbocharging

Roy van Zuijlen * **Frank Kupper** ** **Frank Willems** *,**

* *Eindhoven University of Technology, Faculty of Mechanical Engineering, The Netherlands (e-mail: {r.a.c.zuijlen, f.p.t.willems}@tue.nl)*
** *TNO Automotive, Powertrains Department, Helmond, The Netherlands (e-mail: frank.kupper@tno.nl)*

Abstract: In this paper, Reactivity Controlled Compression Ignition (RCCI) with an electrically-assisted turbocharger (E-turbo) is investigated. This is a promising concept for future green transport, since it can realize very high thermal efficiencies for a wide range of renewable fuels. The combination of RCCI with an E-turbo requires a new approach to manage the energy flows of the engine due to constraints on the storage of electrical energy. The E-turbo shows most potential to increase the engine's thermal efficiency by improved tracking performance of the desired intake conditions. To exploit the full potential of the E-turbo during transients, a dynamic decoupling feedback controller is designed. A supervisory controller based on Pontryagin's Minimum Principle is composed to maximize the brake thermal efficiency while the battery of the E-turbo remains charge sustaining. The supervisory controller determines setpoints for the feedback controller and ensures therefore optimal engine operation during transients. For the simulated, real-world based transient-cycle, fuel savings of 0.64 [%] are realized by the developed supervisory control, while remaining charge sustaining.

Keywords: Engine modelling, engine control, energy management systems, energy control, dynamic decoupling, hybrid vehicles, optimal control.

1. INTRODUCTION

To contribute to solving the problem of global warming, the European Union has formulated a legislation to reduce the CO_2-emissions for heavy-duty vehicles. Compared with 2019, the CO_2-emissions for heavy-duty vehicles should be reduced by 15% in 2025 and by 30% in 2030 (The European Commission, 2019). To comply with this legislation, concepts are investigated, which combine highly efficient advanced combustion concepts with electrification on conventional engines. In this paper, we focus on Reactivity Controlled Compression Ignition (RCCI) with an electrically-assisted turbocharger (E-turbo).

RCCI is an highly efficient combustion concept with ultra-low engine-out NOx- and PM-emissions, where two different types of fuels are used (Reitz and Duraisamy, 2015). This enables the use of a wide range of low carbon and renewable fuels. A low reactivity (gasoline-like) fuel is injected in the intake port outside the combustion chamber and a high reactivity (diesel-like) fuel is directly injected. By varying the quantities and the start of injection of the high reactivity fuel, the combustion process can be controlled. The E-turbo consists of an electric machine, which is installed on the shaft between the Variable Geometry Turbine (VGT) and compressor of the turbocharger. It gives the opportunity to either boost the turbocharger or recuperate energy by adding or storing electric energy in the battery, respectively. The layout of the studied RCCI-engine with E-turbo is shown in Fig. 1, including the Exhaust Gas Recirculation (EGR)-system. Natural Gas (NG) is used as low reactivity fuel and diesel as high reactivity fuel. There are three potential benefits of an E-turbo:

(1) **Enhance overall efficiency** by recuperating exhaust gas energy;
(2) **Increased operating range** in terms of air-fuel ratio;
(3) **Improved transient response of the turbocharger** by boosting.

In this paper, we focus on (3).

With the addition of an E-turbo to the engine layout, a new energy management problem arises. Besides the energy flow of the fuels, the energy level in the battery connected to the E-turbo should be considered. Supervisory control is required to prevent depletion of the battery, such that the E-turbo is always able to assist during transients, and find optimal setpoints for control. In the past, a controller for RCCI-engines with E-turbo is designed in Vlaswinkel et al. (2021), which focused on feedback control of the actuators. However, it lacks a supervisory controller for energy management. Supervisory control strategies are proposed in Song et al. (2019); Zhao et al. (2016, 2019); Zhao et al. (2020) for Diesel engines with E-turbo. Zhao et al. (2016) uses a non-smooth H_∞ synthesis method,

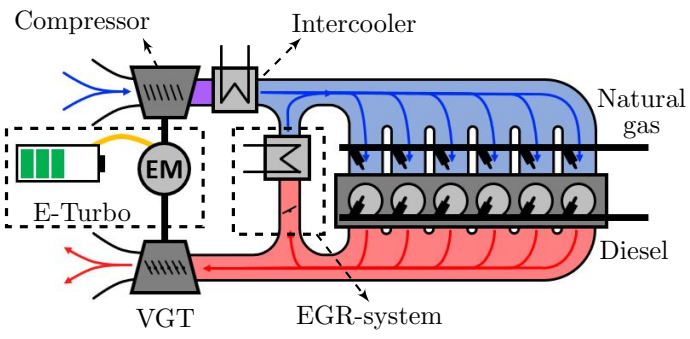

Fig. 1. Layout of the RCCI-engine with E-Turbo.

while Zhao et al. (2019) uses an intuitive approach, which uses the E-turbo for boosting during transients and acts as a generator in stationary conditions to return to the desired energy level in the battery. The supervisory controllers in Song et al. (2019) and Zhao et al. (2020) are based on Model Predictive Control (MPC). The challenges of MPC, however, are the requirement of an highly accurate model and the relatively long computational time. To overcome these challenges, a solution based on Pontryagin's Minimum Principle (PMP) is proposed in this paper. The supervisory controller generates optimal references in terms of the engine's thermal efficiency for feedback control, while being charge sustaining.

This paper is organized as follows: In Section 2, the RCCI-engine with E-turbo is described. The control problem is introduced in Section 3. In Section 4 and 5, the design of the low-level feedback controller and supervisory controller is discussed, respectively. For a World Harmonized Transient Cycle, simulation results are presented in Section 6. Finally, conclusions are drawn and directions for future research are sketched in Section 7.

2. SYSTEM DESCRIPTION

2.1 Engine layout

The studied RCCI engine is based on a 13 liter, 6-cylinder heavy-duty engine. The layout of the engine is depicted in Fig. 1. The air path consists of a turbocharger with compressor and Variable Geometry Turbine (VGT), a cooled, high pressure Exhaust Gas Recirculation (EGR) system and an intercooler. With respect to the baseline EURO-VI Diesel engine, two modifications are done. Firstly, an electric motor-generator, which is connected to a battery, is implemented on the turbocharger shaft. Secondly, the fuel path is modified. In addition to the standard common rail direct injection system for Diesel, a port fuel injection system is added to inject Natural Gas (NG) upstream of the intake valves.

This work focuses on energy management. Therefore, the relevant energy flows for the studied RCCI engine are depicted in Fig. 2. This figure shows the brake power output P_{brake} at the crankshaft and the fuel energy input:

$$\dot{Q}_{\text{fuel}} = \dot{m}_{\text{gas}} \cdot LHV_{\text{gas}} + \dot{m}_{\text{diesel}} \cdot LHV_{\text{diesel}} \tag{1}$$

where $\dot{m}$ is the fuel mass flow and LHV indicates the fuel's lower heating value. Corresponding values are listed in Table 1. The remaining energy flows are discussed in more detail in the modelling part.

2.2 Control-oriented engine model

To model the RCCI engine, the standard mean value engine model, see e.g. (Wahlström and Eriksson, 2011), is adapted. In state space form, the modified engine model is given by:

$$\dot{x} = f(x, u, w, t) \tag{2}$$

with state vector:

$$x^T = [p_{\text{im}}\ T_{\text{im}}\ X_{\text{O,im}}\ p_{\text{em}}\ X_{\text{O,em}}\ \omega_{\text{t}}],$$

where p_{im}, p_{em}, $X_{\text{O,im}}$, and $X_{\text{O,em}}$ are the pressure and oxygen concentration in the intake- and exhaust manifold, respectively. T_{im} denotes the temperature in the intake manifold and ω_{t} is the rotational speed of the turbocharger. The control input vector is given by:

$$u^T = [\dot{m}_{\text{gas}}\ \dot{m}_{\text{diesel}}\ u_{\text{SOI,diesel}}\ u_{\text{EGR}}\ u_{\text{VTG}}\ P_{\text{EM}}],$$

with fuel mass flows $\dot{m}_{\text{gas}}$ and $\dot{m}_{\text{diesel}}$, Diesel injection timing $u_{\text{SOI,diesel}}$, EGR valve and VTG position u_{EGR} and u_{VTG}, and electric machine power P_{EM}. External disturbance vector w includes the engine speed ω_e.

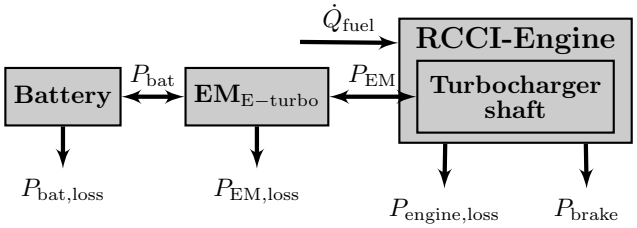

Fig. 2. Main energy flows in the RCCI-engine with E-turbo.

Quadratic polynomial regression models are used to capture the behaviour of the RCCI combustion process within the operating range of interest:

$$y = g(\dot{m}_{\text{f,eqv}}, BR, u_{\text{SOI,diesel}}, \lambda, X_{\text{EGR}}, T_{\text{ivc}}) \tag{3}$$

with:

$$y^T = [IMEP_{\text{g}}\ X_{\text{O,em}}\ T_{\text{evo}}\ p_{\text{evo}}\ CA_{50}],$$

where T_{ivc}, T_{evo} and p_{evo} are the temperatures and pressure at inlet valve closing and exhaust valve opening in the cylinder, respectively. λ is the air/fuel ratio, X_{EGR} is the EGR-rate in the intake manifold, and BR is the energy-based blend ratio (see e.g. (Verhaegh et al., 2022)). BR and equivalent fuel-mass flow $\dot{m}_{\text{f,eqv}}$ are transformations of the fuel mass flows in (1), with $\dot{m}_{\text{f,eqv}} = \dot{m}_{\text{diesel}}/(1 - BR)$. The gross indicated mean effective pressure is denoted with $IMEP_{\text{g}}$, while CA_{50} indicates the combustion phasing. Quadratic polynomials showed sufficient accuracy for control purposes, without overfitting the limited available data. The main model modifications for the E-turbo implementation are discussed in more detail in the sequel.

E-turbo model To describe the effect of the motor-generator on turbocharger dynamics, its power balance is modified in the following way:

$$\frac{d\omega_{\text{t}}}{dt} = \frac{\eta_{\text{m}} P_{\text{t}} - P_{\text{c}} + P_{\text{EM}}}{J_{\text{t}} \omega_{\text{t}}} \tag{4}$$

with turbine power P_{t}, compressor power P_{c}, inertia J_{t}, and the added mechanical power of the electric machine P_{EM}. The mechanical efficiency of the turbocharger, η_{m}, is a function of ω_{t}, u_{VGT}, p_{em}, the post-turbine pressure and the temperature of the electric machine.

Battery model The battery acts as a storage device for energy. The chemical power inside the battery, P_{s}, is modeled with quadratic losses and depends on the electrical power P_{bat}:

$$P_{\text{s}} = \frac{1 - \sqrt{1 - 4\beta P_{\text{bat}}}}{2\beta} \tag{5}$$

with

$$\beta = \frac{R}{n U_{\text{oc}}^2} \tag{6}$$

The used values for the battery parameters can be found in Table 1.

The relation between the electrical battery power P_{bat} and the mechanical power P_{EM} provided by the electric machine at the turbocharger shaft is given by:

$$P_{\text{bat}} = \begin{cases} \eta_{\text{EM}} P_{\text{EM}} & \text{if } P_{\text{EM}} \leq 0; \\ \dfrac{1}{\eta_{\text{EM}}} P_{\text{EM}} & \text{if } P_{\text{EM}} > 0. \end{cases} \tag{7}$$

where $P_{\text{EM}} > 0$ represents the boosting mode and energy is recuperated from the turbocharger for $P_{\text{EM}} \leq 0$.

Table 1. Overview of parameters of the Diesel-Natural Gas RCCI-engine with E-turbo.

Parameter:	Value:	Unit:
Displacement volume (V_d)	13.0	[l]
Number of cylinders (n_cyl)	6	[-]
Lower heating value natural gas (LHV_gas)	38	[MJ/kg]
Lower heating value diesel (LHV_diesel)	42	[MJ/kg]
Electric machine max. power ($P_\mathrm{EM,max}$)	20	[kW]
Electric machine efficiency (η_EM)	95	[%]
Rotational inertia (J_t)	0.77	[g·m^2]
Number of battery cells (n)	250	[-]
Battery internal resistance (R)	0.01	[Ω]
Battery nom. open-circuit cell voltage (U_oc)	3.3	[V]
Battery max. storage capacity ($E_\mathrm{s,max}$)	2.0	[kWh]

Based on the chemical power extracted from the battery, the energy level in the battery (E_s) is given by:

$$E_\mathrm{s}(t) = \int_{t_0}^{t_\mathrm{f}} P_\mathrm{s}(t)\, dt. \tag{8}$$

Then, the state of energy (SoE) is defined as:

$$SoE(t) = \frac{E_\mathrm{s}(t)}{E_\mathrm{s,max}} \cdot 100\% \tag{9}$$

where $E_\mathrm{s,max}$ is the maximum battery storage capacity.

3. CONTROL PROBLEM

In order to design a controller for the RCCI-engine with E-turbo, the control problem is formulated. First the high-level control objectives are given, followed by the control architecture. The section concludes with the controlled outputs used in the controller.

3.1 High-level control objectives

The RCCI engine controller aims to realize the requested engine torque with maximal overall energy efficiency, while meeting constraints for safe operation and for tailpipe emissions. For RCCI engines, safe and stable operation is challenging (Paykani et al., 2021); this advanced combustion concept is sensitive for changing operating conditions. Consequently, the RCCI engine controller needs to avoid misfires at low load operation and to avoid damage associated with unacceptable peak in-cylinder pressure and pressure rise rates at high load.

3.2 Control architecture

The control architecture to achieve the control objectives, is given in Fig. 3. The controller consists of two parts; the supervisory controller and the feedback controller. The supervisory controller determines references for the feedback controller, depending on the engine speed ω_e and torque request τ_e. A part of the supervisory controller is the energy management for the energy level in the battery. The feedback controller ensures that the references are tracked, under disturbances d and measurement noise m.

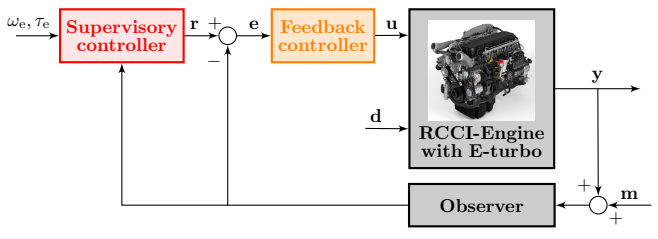

Fig. 3. Engine control architecture for RCCI-engine with E-turbo.

3.3 Selected controlled outputs

To reach the control objectives with the control inputs of (10), an appropriate selection of controlled outputs has to be made. To maximize the overall engine efficiency, the combustion phasing CA_{50} is used as controlled output to be able to maintain the optimal combustion phasing. The pressure difference dp across the engine is selected due to its relation with the pumping losses and air-fuel ratio λ to have precise control of the amount of air. Furthermore, it turned out that air-path actuators u_VGT and P_EM have good controllability of dp and λ, which makes them suitable as controlled outputs. With the gross indicated mean effective pressure $IMEP_\mathrm{g}$, the power output of the engine can be controlled. Within the investigated operating range, safety constrains are not violated. The controlled outputs $\mathbf{r}$ become, therefore:

$$\mathbf{r}^T = [IMEP_\mathrm{g}\ CA_{50}\ dp\ \lambda]\,.$$

where $dp = p_\mathrm{em} - p_\mathrm{im}$.

4. FEEDBACK CONTROLLER

As feedback controller, a dynamic decoupling feedback control structure is developed to cope with the different dynamics of the VGT and E-turbo and meet the control objectives defined in Section 3.1. The main purpose of the feedback controller is tracking the defined references as close as possible and reject disturbances. Since the references are selected such that maximum brake thermal efficiency is achieved, any deviation from these references results in sub-optimal engine operation. For feedback control, we will use the following control inputs:

$$\mathbf{u}^T = [\dot{m}_\mathrm{gas}\ \dot{m}_\mathrm{diesel}\ u_\mathrm{VGT}\ P_\mathrm{EM}]$$

Two control inputs $u_\mathrm{SOI,diesel}$ and u_EGR are disregarded from the feedback controller due to their lack of controllability for given $\mathbf{r}$ and will be controlled open-loop.

Since the E-turbo acts directly on the turbocharger dynamics while the VGT lags due to the air-path dynamics, the two control inputs have strongly different dynamics on the controlled outputs dp and λ. To overcome this challenge, we use a dynamic decoupling feedback control structure, as can be seen in Fig. 4. The feedback controller consists of controller $\mathcal{C}(s)$ and decoupler $\mathcal{D}(s)$.

The dynamic decoupling $\mathcal{D}(s)$ takes the dynamics of the system into account and inverses the system over its complete frequency domain:

$$\mathcal{D}(s) = \mathcal{H}^{-1}(s). \tag{10}$$

$\mathcal{H}(s)$ is identified by multisine system identification at one operating point.

To prevent inverting couplings that are not or barely present, some couplings are set to 0. Based on the system identification, the couplings that are set to 0 are fuel-path control inputs $\dot{m}_\mathrm{gas}$ and $\dot{m}_\mathrm{diesel}$ to dp and the air-path control inputs u_VGT and P_EM to $IMEP_\mathrm{g}$ and CA_{50}.

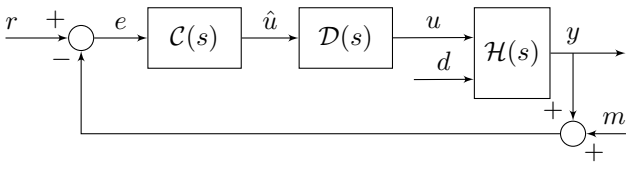

Fig. 4. Dynamic decoupling feedback control structure with dynamic decoupler $\mathcal{D}(s)$.

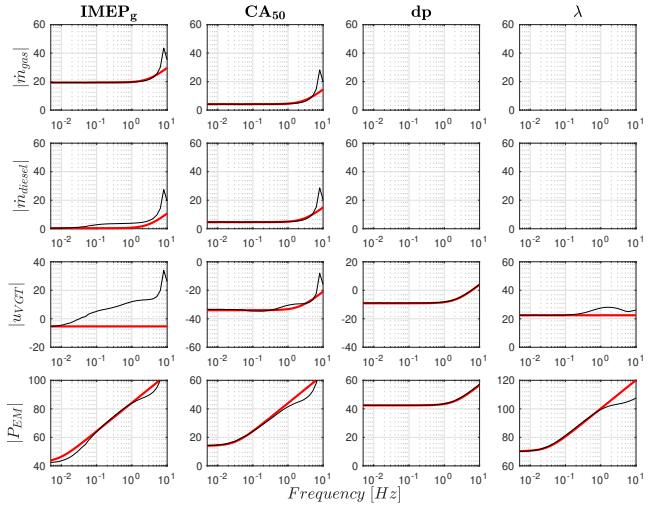

Fig. 5. Dynamic decoupling estimations of inverse plant at $\omega_e = 1000$ [RPM] and $\dot{m}_{f,eqv} = 130$ [mg/inj].

Based on this information, decoupler $\mathcal{D}(s)$ has following structure:

$$\mathcal{D}(s) = \begin{bmatrix} d_{11}(s) & d_{12}(s) & 0 & 0 \\ d_{21}(s) & d_{22}(s) & 0 & 0 \\ d_{31}(s) & d_{32}(s) & d_{33}(s) & d_{34}(s) \\ d_{41}(s) & d_{42}(s) & d_{43}(s) & d_{44}(s) \end{bmatrix}. \quad (11)$$

Each term $d_{ij}(s)$ within matrix $\mathcal{D}(s)$ is estimated based on first-order functions:

$$d_{ij}(s) = k_c + k_d \cdot s \quad (12)$$

where k_c and k_d are manually selected to estimate $\mathcal{D}(s)$. The inverses of the frequency responses up until the highest frequency possible are fitted with minimal error in magnitude. In Fig. 5 the frequency responses and their estimation are visualized.

Feedback controller $\mathcal{C}(s)$ has following structure:

$$\mathcal{C}(s) = \text{diag}\,(c_1(s),\ c_2(s),\ c_3(s),\ c_4(s)) \quad (13)$$

where $c_i(s)$ are individual feedback controllers. $c_i(s)$ consists of a PI-controller in combination with a first- and second-order low-pass filter:

$$c_i(s) = K_p \left(1 + \frac{K_i}{s}\right) \cdot \frac{1}{\frac{1}{2\pi f_{lp1}} s + 1} \cdot \frac{1}{\frac{1}{(2\pi f_{lp2})^2} s^2 + \frac{1.4}{2\pi f_{lp2}} s + 1} \quad (14)$$

where K_p and K_i are the tuning gains for the PI-controller, and f_{lp1} and f_{lp2} are the frequencies for the first-order and second-order low-pass filters respectively. The filters are required to avoid high gains at high frequencies, which are amplified by the derivative terms of (12).

Table 2. Gains of controller $\mathcal{C}(s)$ and the resulting design criteria for the closed-loop system at $\omega_e = 1000$ [RPM] and $\dot{m}_{f,eqv} = 130$ [mg/inj]..

Controller:	**IMEP$_g$** $c_1(s)$	**CA$_{50}$** $c_2(s)$	**dp** $c_3(s)$	λ $c_4(s)$
Gains:				
K_p [-]	0.5	0.5	0.6	0.6
K_i [-]	10	10	10	10
f_{lp1} [Hz]	2	2	1	1
f_{lp2} [Hz]	3	3	not present	3
Design criteria:				
ω_{co} [Hz]	0.8	0.8	0.8	0.8
MM [dB]	3.6	3.9	2.3	3.0
PM [°]	70.9	68.4	46.8	79.7

A bandwidth (ω_{co}) of 0.8 [Hz] is achieved for all four feedback controllers. This is done by loop shaping, following the same approach as in Verhaegh et al. (2022). The bandwidth is defined as the open-loop cross-over frequency, where $|\mathcal{CDH}| = 0$ [dB]. The targeted stability margin is a modulus margin (MM) of maximal 6 [dB]. All controllers are designed such that the phase margin (PM) is at least 30 [°], see Table 2. Furthermore the generalized Nyquist criteria is evaluated to guarantee stability of the closed loop MIMO system.

5. SUPERVISORY CONTROLLER

Figure 6 shows the proposed supervisory control architecture for energy management. In the control input vector $\mathbf{u}(t)$ there are four actuators. The two fuelling inputs are used to track r_{IMEP_g} and $r_{CA_{50}}$. The remaining u_{VTG} and P_{EM} are available in the supervisory controller to ensure that the energy level in the battery is charge sustaining, while minimizing the fuel consumption. From Fig. 7, it is concluded that λ and dp can be independently controlled using u_{VTG} and P_{EM}. This figure also clearly illustrates the potential increase of the operating range due to the E-turbo in the studied operating point. The optimal settings corresponding to minimum fuel consumption, and thus maximal overall engine efficiency, are indicated by the pink line in Fig. 7. Furthermore, this figure illustrates that an increased P_{EM} results in decreased fuel consumption. This reduction is associated with reduced pumping losses. Note that battery SoE is not taken into account.

As illustrated in Fig. 6, a three step approach is followed to guarantee optimal performance:

(1) For each engine operating point (ω_e, P_{brake}), an optimal VTG position u^*_{VTG} is determined by off-line optimization. This setting is optimal for a specified P_{EM}, as illustrated in Fig. 7;
(2) Selected u^*_{VTG} is input to the optimal control problem to determine the fuel-optimal P^*_{EM};
(3) Based on the selected u^*_{VTG} and P^*_{EM}, the corresponding references for r_{dp} and r_λ are determined from Fig. 7.

Within the investigated operating range, the designed feedback control in Section 4 was sufficient in terms of stability. To accomplish stability for a larger operating range, a dense grid of local feedback controllers is required.

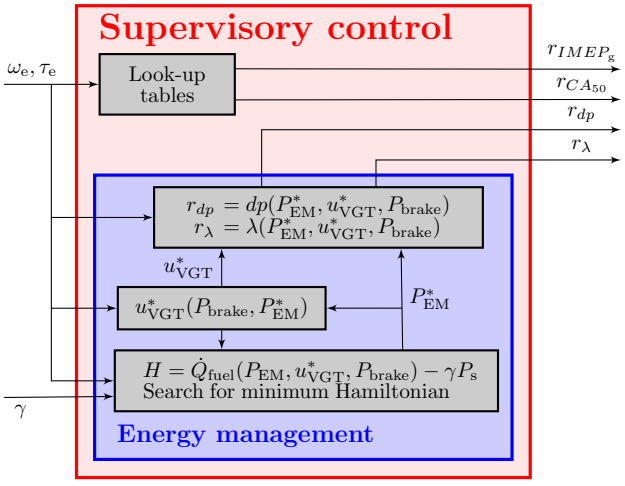

Fig. 6. Supervisory controller structure. References r are input for the feedback controller designed in Section 4.

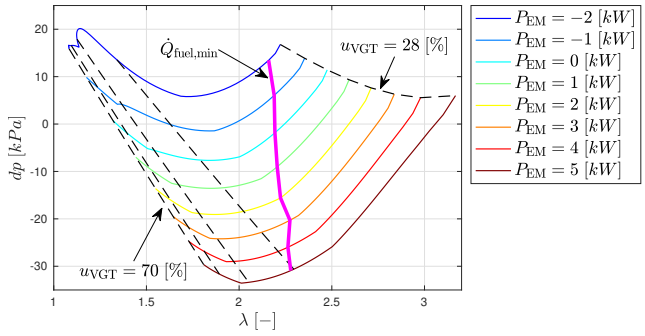

Fig. 7. Controllability of dp and λ using u_{VGT} and P_{EM}. Purple line indicates operational settings for minimal fuel consumption at P_{brake}=130 kW.

5.1 Optimal control problem

For energy management, the optimization problem is formulated as follows:

$$\min_{u(t)} J = \int_{t_0}^{t_f} \dot{Q}_{\text{fuel}}(P_{\text{EM}}, u^*_{\text{VGT}}, P_{\text{brake}})dt \tag{15a}$$

such that:

$$\dot{E}_{\text{s}}(t) = P_{\text{s}}(t) \tag{15b}$$
$$E_{\text{s}}(t_{\text{f}}) = E_{\text{s}}(t_0) \tag{15c}$$

with decision variable $u(t) = P_{\text{EM}}(t)$. As specified by (15c), we aim for a charge sustaining solution over the studied time window.

5.2 Optimal solution

The optimization problem of (15) is solved using Pontryagin's Minimum Principle (PMP). Based on (15), the Hamiltonian H can be written as:

$$H = \dot{Q}_{\text{fuel}}(P_{\text{EM}}, u^*_{\text{VGT}}, P_{\text{brake}}) - \gamma \frac{1 - \sqrt{1 - 4\beta P_{\text{bat}}}}{2\beta} \tag{16}$$

To find the optimal control inputs $u^*(t)$, two necessary conditions are given using PMP. Firstly, the following equation can be derived for the co-state γ :

$$\dot{\gamma}^*(t) = \frac{\partial H}{\partial E_{\text{s}}} = 0 \tag{17}$$

As a result, the optimal input corresponds to a constant co-state value. Solving the second necessary condition ($\frac{\partial H}{\partial P_{\text{EM}}}$=0) gives:

$$\begin{aligned} 0 = & \frac{\partial \dot{Q}_{\text{fuel}}(P_{\text{EM}}, u^*_{\text{VGT}}, P_{\text{brake}})}{\partial P_{\text{EM}}} \\ & -\gamma \frac{\partial(\frac{1-\sqrt{1-4\beta P_{\text{bat}}}}{2\beta})}{\partial P_{\text{bat}}} \cdot \frac{\partial P_{\text{bat}}}{\partial P_{\text{EM}}} \end{aligned} \tag{18}$$

The supervisory control should ensure that the engine always operates on the optimal fuel consumption line, whereby variations in P_{EM} are allowed to end up with a charge sustaining strategy. For each P_{brake} and P_{EM}, the stationary optimal control input u^*_{VGT} is determined (see step 1). By evaluating the complete operating range, $u^*_{\text{VGT}}(P_{\text{brake}}, P_{\text{EM}})$ is derived. This is stored in a look-up table or described by a regression model.

6. SIMULATION RESULTS

To assess the potential of the designed controller, simulations are performed for a real-world scenario based on a World Harmonized Transient Cycle (WHTC). Due to model limitations, the original WHTC has been modified: ω_{e} is fixed at 1000 [RPM] and $IMEP_{\text{g}}$ is clipped between 8 and 20 [bar]. Two aspects are studied: the effect of the E-turbo on transient performance and the potential of energy management. Therefore, the following three cases are studied:

(1) Without E-turbo.
(2) With E-turbo, without energy management.
(3) With E-turbo, with energy management.

References $\mathbf{r}$ are operating point dependent setpoints and are determined by off-line optimization with $P_{\text{EM}} = 0$ [kW] for cases 1 and 2. For case 3, $r_{CA_{50}}$ and $r_{IMEP_{\text{g}}}$ are the same as in case 1 and 2, while r_{dp} and r_λ are determined by the supervisory controller (see also Fig.6). The overall cycle results are summarized in Table 3.

6.1 E-turbo effect on transient performance

In Fig. 8, the results of Case 1 and 2 are shown. It is seen that application of the E-turbo reduces substantially the tracking error e_{dp} and e_λ. The mean absolute tracking $\bar{e}_{\text{abs},dp}$ and $\bar{e}_{\text{abs},\lambda}$ over the complete cycle decreases by 95.0 and 92.3 [%] respectively, see Table 3. Analysing the control inputs learns that the E-turbo is predominantly active during transients, while the slow air path dynamics are captured by the VGT. By boosting ($P_{\text{EM}} > 0$) or energy recuperation ($P_{\text{EM}} < 0$) with the E-turbo, more direct control of λ and dp is feasible via relative fast changes in turbocharger speed. Consequently, r_λ and r_{dp}, which are associated with optimal combustion, are tracked more closely in Case 2. This leads to a decrease in total fuel consumption ($m_{\text{gas}} + m_{\text{diesel}}$), as illustrated in the bottom right-hand figure for Case 2 compared to Case 1.

To assess the overall energy efficiency benefit, the corrected cumulative brake specific fuel consumption is introduced, which compensates for the change in SoE:

$$BSFC_{\text{cor}}(t) = \frac{\int_0^t (\dot{m}_{\text{diesel}}(t) + \dot{m}_{\text{gas}}(t))\, dt}{\int_0^t (P_{\text{brake}}(t) - P_{\text{s}}(t))\, dt} \tag{19}$$

where $P_{\text{s}}(t)$ is the chemical power of the battery as in (5). When energy is distracted from the battery over the cycle, the term $P_{\text{brake}} - P_{\text{s}}$ increases, so $BSFC_{\text{cor}}$ is reduced for the same fuel input. From Table 3, it is concluded that $BSFC_{\text{cor}}$ is reduced by 0.61 [%] in Case 2. However, this is realized while depleting the battery from SoE=50% to 39.45%. This emphasizes the need for a supervisory control with energy management in order to end up with a charge sustaining strategy.

6.2 Potential of energy management

In Fig. 9, simulation results are shown for the supervisory controller (Case 3). These results are compared with Case 2 (without energy management). The co-state γ is found by manual tuning and is fixed at -1.48 to end

Table 3. Comparison of cycle results for tracking performance, SoE and $BSFC_{\text{cor}}$.

	Case 1	**Case 2**	**Case 3**
$\bar{e}_{\text{abs},IMEP_{\text{g}}}$ [bar]	0.297	0.169 (-43.1%)	0.169 (-43.1%)
$\bar{e}_{\text{abs},CA_{50}}$ [°CA]	0.130	0.091 (-30.0%)	0.094 (-27.7%)
$\bar{e}_{\text{abs},dp}$ [kPa]	15.542	0.780 (-95.0%)	1.315 (-91.5%)
$\bar{e}_{\text{abs},\lambda}$ [-]	0.130	0.010 (-92.3%)	0.010 (-92.3%)
$\Delta SoE(t_{\text{f}})$ [%]	-	-10.55	+3.99
$BSFC_{\text{cor}}(t_{\text{f}})$ [g/kWh]	178.03	176.94 (-0.61%)	176.89 (-0.64%)

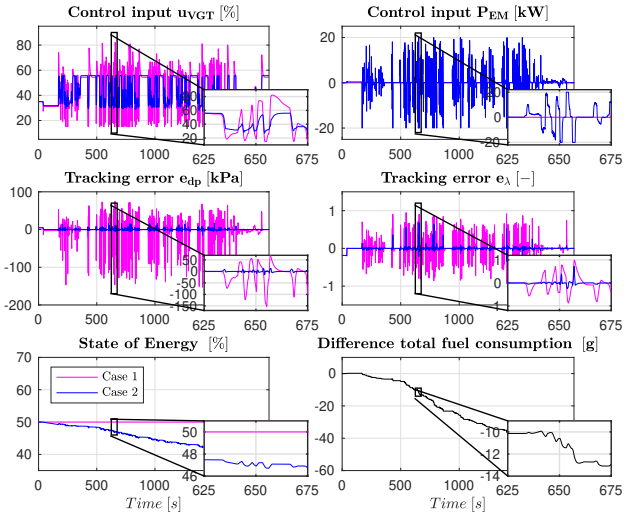

Fig. 8. Comparison of Case 1 and 2 with $\omega_e = 1000$ [RPM], $u_{EGR} = 0$ [%] and $u_{SOI,diesel} = -80$ [°CAaTDC].

up with a close to charge sustaining strategy over the simulated cycle. The supervisory controller determines different references for dp and λ compared to Case 1 and 2; these fuel optimal settings are found by moving over the purple line in Fig. 7 for varying P_{EM}. This results in reduced new control inputs u_{VGT}. As illustrated in the bottom left-hand figure, up to t=170 [s] the battery is charged for the selected co-state setting. This corresponds to a higher setpoint r_{dp} and a lower setpoint r_λ. After this initial phase, battery charging and depleting is balanced over the remaining part of the cycle. Due to these new control inputs, a strategy close to charge sustaining is obtained. However, the charging of the battery is at the cost of fuel. The bottom right-hand figure shows the increased total fuel consumption in Case 3 compared to Case 2. From this figure, it is concluded that the optimal setpoints selected by the supervisory controller are less fuel efficient than for $P_{EM} = 0$ (Case 2). Over the cycle, a cumulative $BSFC_{cor}$ of 176.89 [g/kWh] is found, which is nearly identical to the result in Case 2. This is mainly due to the correction for the energy level in the battery in (19). Comparing Case 3 with Case 1 shows that the E-turbo with supervisory controller is able to reduce the cumulative $BSFC_{cor}$ with 0.64 [%], while the battery is not depleted.

7. CONCLUSIONS AND FUTURE RESEARCH

In this paper, a new energy management strategy is presented for RCCI-engines with E-turbo. Where earlier work on RCCI-control focused on feedback control, this work considers both supervisory and feedback control. The controller consists of a dynamic decoupled feedback controller to cope with the different dynamics of the VGT and E-turbo, and a PMP-based supervisory controller to obtain a charge sustaining strategy. It is shown that the addition of an E-turbo results in a decrease in fuel consumption of 0.64 [%] over the studied cycle. This is mainly caused by the improved transient response during boosting as well as energy recuperation. Whether similar results can be achieved on an actual engine set-up with disturbances and uncertainties is part of future work. With energy management, it is possible to obtain a charge sustaining strategy without increasing the fuel consumption. Further research will focus on extending the model and controller to deal with the whole operating range of the engine.

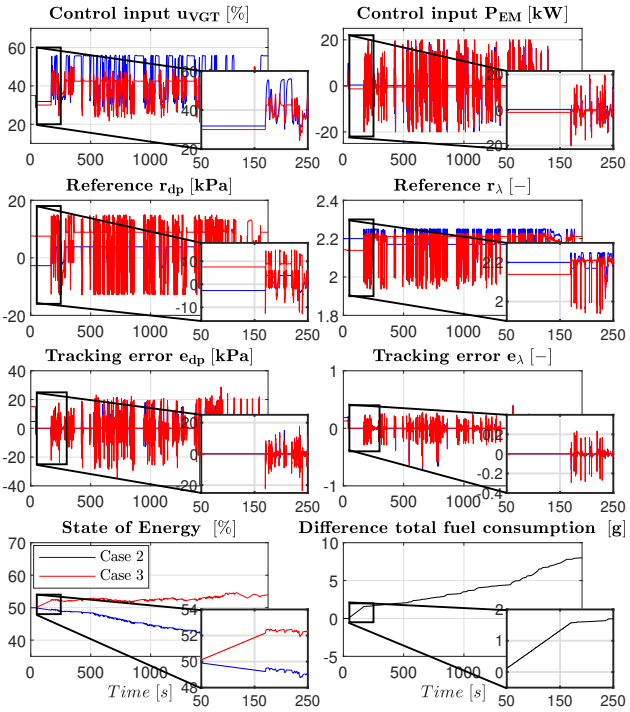

Fig. 9. Comparison of Case 2 and 3. with $\omega_e = 1000$ [RPM], $u_{EGR} = 0$ [%] and $u_{SOI,diesel} = -80$ [°CAaTDC].

REFERENCES

Paykani, A., Garcia, A., Shahbakhti, M., Rahnama, P., and Reitz, R.D. (2021). Reactivity controlled compression ignition engine: Pathways towards commercial viability. *Applied Energy*, 282, 116174. doi:10.1016/j.apenergy.2020.116174.

Reitz, R.D. and Duraisamy, G. (2015). Review of high efficiency and clean reactivity controlled compression ignition (RCCI) combustion in internal combustion engines. *Progress in Energy and Combustion Science*, 46, 12–71.

Song, K., Upadhyay, D., and Xie, H. (2019). Control of diesel engines with electrically assisted turbocharging through an extended state observer based nonlinear MPC. *Proceedings of the Institution of Mechanical Engineers, Part D: Journal of Automobile Engineering*, 233(2), 378–395.

The European Commission (2019). CO2 emission performance standards for new heavy-duty vehicles.

Verhaegh, J., Kupper, F., and Willems, F. (2022). Data-driven air-fuel path control design for robust rcci engine operation. *Energies*, 15(6).

Vlaswinkel, M., de Jager, A., and Willems, F. (2021). Data-based control structure selection for RCCI engines with electrically assisted turbocharger. In *Proceedings of the 19th European Control Conference (ECC 2021)*, 491–496. European Union Control Association (EUCA).

Wahlström, J. and Eriksson, L. (2011). Modelling diesel engines with a variable-geometry turbocharger and exhaust gas recirculation by optimization of model parameters for capturing non-linear system dynamics. *Proceedings of the Institution of Mechanical Engineers, Part D: Journal of Automobile Engineering*, 225(7), 960–986. doi:10.1177/0954407011398177.

Zhao, D., Gu, W., and Mason, B. (2019). Real time energy management of electrically turbocharged engines based on model learning. In *WCX SAE World Congress Experience*. SAE International. doi:https://doi.org/10.4271/2019-01-1056.

Zhao, D., Stobart, R., and Mason, B. (2020). Real-time energy management of the electric turbocharger based on explicit model predictive control. *IEEE Transactions on Industrial Electronics*, 67(4), 3126–3137.

Zhao, D., Winward, E., Yang, Z., Stobart, R., and Steffen, T. (2016). Real-time optimal energy management of electrified engines. *IFAC-PapersOnLine*, 49(11), 251–258. 8th IFAC Symposium on Advances in Automotive Control AAC 2016.